

THE (UNSTABLE) THRESHOLD OF BLACK HOLE FORMATION

M.W. CHOPTUIK

Center for Relativity

Dept. of Physics

*The University of Texas at Austin
Austin TX, 78712-1081*

1. Introduction

In recent years it has become apparent that intriguing phenomenology exists at the threshold of black hole formation in a large class of general relativistic collapse models. This phenomenology, which includes scaling, self-similarity and universality, is largely analogous to statistical mechanical critical behaviour, a fact which was first noted empirically, and subsequently clarified by perturbative calculations which borrow on ideas and techniques from dynamical systems theory and renormalization group theory. This contribution, which closely parallels my talk at the conference, consists of an overview of the considerable “zoo” of critical solutions which have been discovered thus far, along with a brief discussion of how we currently understand the nature of these solutions from the point of view of perturbation theory. The reader who wishes additional details concerning the subject is referred to Gundlach’s excellent recent review [1]. Earlier synopses by Evans [2] and Eardley [3] may also be of interest. Finally, those readers interested in the relationship of black-hole critical phenomena to questions of cosmic censorship—a topic which is *not* discussed below—can consult Wald’s recent discussion of the status of cosmic censorship [4].

2. Critical Behaviour in Massless Scalar Collapse

I begin with a fairly detailed description of critical behaviour in the self-gravitating dynamics of a spherically-symmetric, massless scalar field. Apart from historical reasons, I do so, not only because it is arguably the simplest “realistic” model of gravitational collapse, but, more importantly, because

most of the features we currently associate with critical collapse can be seen in the model.

2.1. EQUATIONS OF MOTION

Adopting the usual spherical coordinates (t, r, θ, φ) , and geometric units, $G = c = 1$, the spherically-symmetric spacetime metric can be written

$$ds^2 = -\alpha^2(r, t) dt^2 + a^2(r, t) dr^2 + r^2 (d\theta^2 + \sin^2 \theta d\varphi^2). \quad (1)$$

The coordinate system I have thus adopted is a natural generalization of Schwarzschild coordinates—in numerical relativity parlance it is the polar-areal (or polar-radial) system. Note that the radial coordinate, r , measures proper surface area and thus has an immediate geometric interpretation. The time coordinate, t , on the other hand, has no particular physical significance. However, from the point of view of critical phenomena, there is a preferred labeling (reparametrization) of the $t = \text{constant}$ surfaces, namely the one given by the proper time, $T_0(t)$, of an observer at rest at $r = 0$:

$$T_0(t) \equiv \int_0^t \alpha(0, \tilde{t}) d\tilde{t}. \quad (2)$$

Defining auxiliary scalar field variables, Φ and Π :

$$\Phi(r, t) \equiv \frac{\partial \phi}{\partial r}(r, t), \quad (3)$$

$$\Pi(r, t) \equiv \frac{a}{\alpha} \frac{\partial \phi}{\partial t}(r, t), \quad (4)$$

a sufficient set of equations for the EMKG (Einstein-massless-Klein-Gordon) model is

$$\frac{\partial \Phi}{\partial t} = \frac{\partial}{\partial r} \left(\frac{\alpha}{a} \Pi \right), \quad (5)$$

$$\frac{\partial \Pi}{\partial t} = \frac{1}{r^2} \frac{\partial}{\partial r} \left(r^2 \frac{\alpha}{a} \Phi \right), \quad (6)$$

$$\frac{1}{\alpha} \frac{d\alpha}{dr} - \frac{1}{a} \frac{da}{dr} + \frac{1 - a^2}{r} = 0, \quad (7)$$

$$\frac{1}{a} \frac{da}{dr} + \frac{a^2 - 1}{2r} - 2\pi r (\Pi^2 + \Phi^2) = 0. \quad (8)$$

Here (7) is the *slicing condition* which constrains the lapse function, α , at all instants of time, and (8) is the *Hamiltonian constraint* which similarly constrains the radial metric function a .

It is useful to discuss the dynamics of the scalar field in terms of further auxiliary variables, X and Y , defined by

$$X(r, t) \equiv \sqrt{2\pi} \frac{r}{a} \Phi = \sqrt{2\pi} \frac{r}{a} \frac{\partial \phi}{\partial r}, \quad (9)$$

$$Y(r, t) \equiv \sqrt{2\pi} \frac{r}{a} \Pi = \sqrt{2\pi} \frac{r}{a} \frac{\partial \phi}{\partial t}. \quad (10)$$

Note that the equations of motion (5)–(8) are invariant under the trivial rescalings $r \rightarrow kr$, $t \rightarrow kt$, for arbitrary $k > 0$, and that X and Y are form-invariant under such transformations. It is also convenient to introduce the *mass aspect* function, $m(r, t)$, defined in analogy with the usual Schwarzschild form of the static spherically-symmetric metric:

$$a^2(r, t) = \left(1 - \frac{2m(r, t)}{r}\right)^{-1}. \quad (11)$$

In terms of the X and Y variables, $dm/dr = X^2 + Y^2$, and the total mass (ADM mass), M_{ADM} , of the spacetime is given by

$$M_{\text{ADM}} = \int_0^\infty \frac{dm}{dr} dr = \int_0^\infty X^2 + Y^2 dr. \quad (12)$$

Another useful relationship expresses the spacetime curvature scalar, R , as a function of X and Y :

$$R = -8\pi T = 8\pi \nabla^\mu \phi \nabla_\mu \phi = \frac{4}{r^2} (X^2 - Y^2). \quad (13)$$

where T is the trace of the scalar field stress-energy tensor.

As is well known, polar-areal coordinates cannot cross apparent horizons, and thus, for the most part, cannot penetrate event horizons. However, black hole formation is clearly signaled in a calculation (see Figure 1) by (among other things)

$$\frac{2m}{r} \Big|_{R_{\text{BH}}} \rightarrow 1, \quad (14)$$

at some radius $r = R_{\text{BH}}$ from which the mass, $M_{\text{BH}} = R_{\text{BH}}/2$, of the final black hole can be quite accurately estimated.

2.2. COMPETITION AND THE THRESHOLD OF BH FORMATION

At a heuristic level, the existence of critical behaviour in the EMKG system and other models is a direct result of *competition* in the dynamics. The nature of this competition can be seen by addressing the question: “given

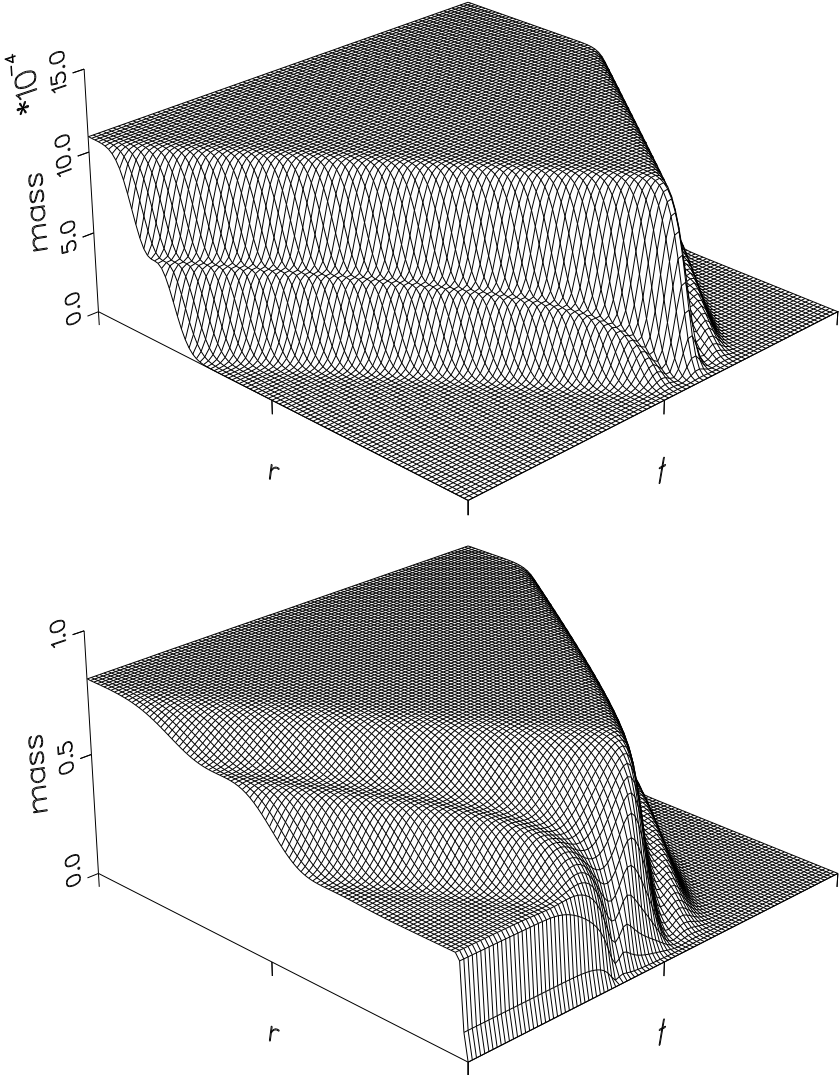


Figure 1. Behaviour of the mass aspect function, $m(r, t)$, for cases of complete dispersal (top), and black hole formation (bottom), in massless scalar collapse. The origin, $(0, 0)$, in both plots is at the extreme right. Initial data in both cases is a single ingoing Gaussian profile— $\phi(r, 0) = p g(r)$ —the calculations differ only in the choice of the overall amplitude factor, p , which is sub-critical ($p < p^*$) in the first instance, and super-critical ($p > p^*$) in the second. Note that flat regions in the plots are vacuum. In the sub-critical case, the scalar field implodes through the origin, then completely disperses leaving (essentially) flat spacetime in its wake. In the super-critical case, the scalar field again implodes through the origin, but now forms a black hole containing roughly half of the total mass of the spacetime. Dynamically, the geometry within the dispersing (outgoing) scalar field settles down to an exterior-Schwarzschild solution on a time scale set by the size of the hole, $T \sim R_{\text{BH}} = 2M_{\text{BH}}$.

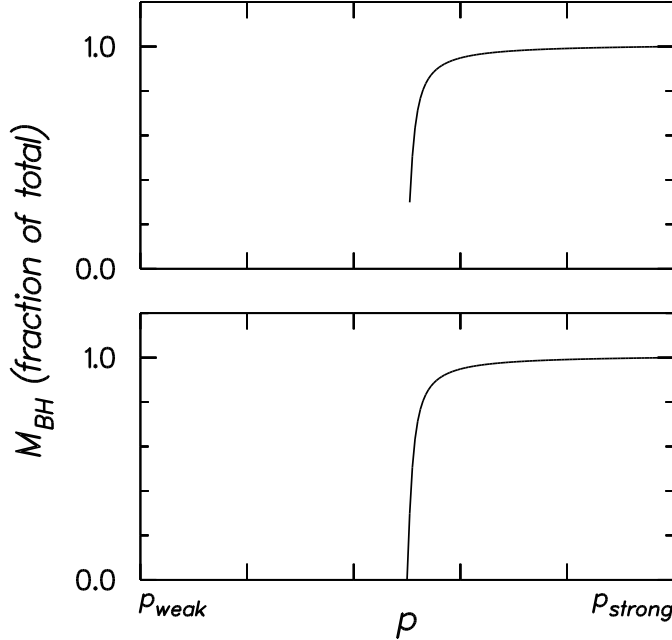


Figure 2. Schematic illustration of black-hole-threshold possibilities. The top panel represents a first-order (Type I) transition, where the “order parameter” (the black hole mass) exhibits a gap at threshold, while the bottom panel shows a second-order (Type II) transition, where the black hole mass is infinitesimal at the critical point.

generic initial data representing an imploding pulse (shell) of scalar radiation, where can the energy in the system end up at late times?” Roughly speaking, the kinetic energy of the massless field wants to disperse the field to infinity, whereas the gravitational potential energy (entirely self-induced), if sufficiently dominant during the collapse, will result in the trapping of some amount of the mass-energy of the system in a black hole. Indeed, the fact that, for *generic* initial data, there *are* only these two qualitatively distinct end-states in the model has been rigorously established by Christodoulou [5, 4]. However, empirical evidence (i.e. direct solution of the equations of motion) rapidly leads one to the same conclusion. The key point is that the dynamical competition can be controlled by tuning a parameter in the initial conditions: it is an easy matter to set up families of initial data, $\{\Phi(r, 0; p), \Pi(r, 0; p)\}$ such that if the parameter, p , is less than some critical (threshold) value, p^* , the scalar field completely disperses, while if $p > p^*$ a black hole forms (Figure 1).

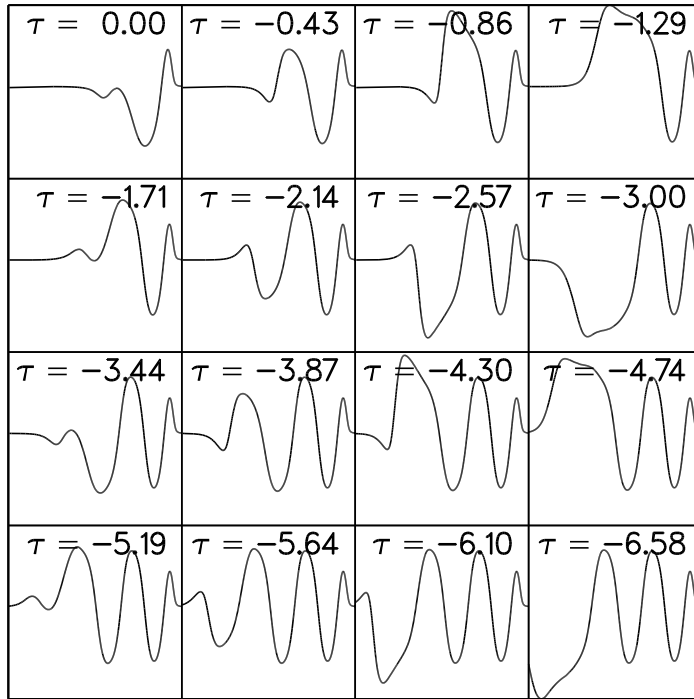


Figure 3. Near-critical evolution of the auxiliary scalar field variable, X (see equation (9)), in massless scalar collapse. Evolution proceeds left-to-right, top-to-bottom. In each frame, X is plotted versus the logarithmic radial coordinate, $\rho \equiv \ln r$, with displayed ordinate values ranging from -0.37 to 0.33. Constant increments of logarithmic time, $\tau \equiv \ln(T_0^* - T_0)$, separate each successive snapshot. The discrete self-similarity of the critical solution can be clearly seen by comparing the trailing (left-most) edges of pairs of waveforms separated by two rows in the plot. Each such pair is very nearly in the same “phase” of critical evolution, but the dynamics of the later frame (more negative τ) is occurring on a scale some $\exp(\Delta) \approx 30$ times smaller than that of the earlier snapshot. Note that the leading parts of the waveforms (the roughly sinusoidal oscillations) are almost purely-outgoing, and do not, *per se*, constitute part of the critical dynamics. The fact that these oscillations appear to be “frozen”, rather than propagating, is a result of the fact that the time between successive frames is exponentially decreasing. At any scale (position along the horizontal axis) of the critical evolution, there are three basic possibilities: (1) if the evolution is sub-critical (at that scale), the scalar field will completely disperse, (2) if the evolution is super-critical, a black hole *with a size set by the current scale of the critical dynamics* will form, and (3) if the evolution is precisely-critical, the strong field evolution will continue to a smaller scale. This behaviour provides convincing evidence for a Type II transition in the model. Plots of the other scalar field variable, Y , as well as $X^2 + Y^2 = dm/dr$ and $X^2 - Y^2 = 4R/r^2$ show analogous oscillatory behaviour between fixed limits. Since the strong-field regime is characterized by $r \rightarrow 0$ for a precisely critical solution, this last fact shows immediately that the spacetime scalar curvature, R , diverges in the critical limit.

The existence of interpolating families and black hole thresholds in the EMKG model was well-established in early studies of the system [6, 7, 8]. The discovery of critical behaviour in the model, however, came later, and was a direct result of a question Christodoulou posed in 1987 [9]: “will black hole formation turn on at *finite* or *infinitesimal* mass for a generic interpolating family at threshold?” (see Figure 2). Viewing the black-hole mass as an order parameter, I refer to these two possibilities as Type I and Type II transitions, respectively, in analogy with first and second order phase transitions in statistical mechanical systems.

2.3. TYPE II BEHAVIOUR IN THE EMKG MODEL

Detailed phenomenological studies [10, 11, 12] using many initial data families clearly demonstrated that the strong-field (i.e. critical) dynamics in the EMKG model is characterized by an essentially *unique* solution of the equations of motion, which I denote schematically as Z^* . Like the Schwarzschild solution, Z^* , is only determined upto an overall (length/time) scale, but unlike Schwarzschild, the critical solution is obviously (by construction!) *unstable*—the slightest perturbation will result in either complete dispersal or black hole formation.

A key feature of the critical solution (and of all currently known Type II solutions) is *self-similarity* or *scale invariance*—loosely speaking, the critical solution has a scale (homothetic) Killing vector. (Correspondingly, the known Type I critical solutions discussed in section 6 are characterized by timelike Killing vectors). Empirically, this means as one tunes closer and closer to a critical point one sees, in a single evolution, the same strong-field dynamics playing out on a wider and wider range of spatial scales, always in a (shrinking) neighborhood of $r = 0$. In the scalar field case (see Figure 3), the dynamics at any particular “scale epoch” is decidedly non-trivial—i.e. the self-similarity is *discrete*, rather than continuous. This novel “echoing” feature of the solution, whereby the dynamics repeats on scales related by a factor of e^Δ , $\Delta = 3.44\dots$, is one of the most intriguing aspects of the solution, and its origin remains somewhat of a mystery. We can express the discrete self-similarity in slightly more mathematical terms by noting that in a precisely critical evolution, the strong-field evolution “accumulates” at a singular event with (r, T_0) coordinates $(0, T_0^*)$. Then defining logarithmic coordinates, $\rho \equiv \ln r$, $\tau \equiv \ln(T_0^* - T_0)$, we have

$$Z^*(\rho \pm n\Delta, \tau \pm n\Delta) \sim Z^*(\rho, \tau) \quad n = 0, 1, 2, \dots \quad (15)$$

As explained in more detail in Figure 3, the nature of the critical dynamics (which is now well-understood, albeit in a non-rigorous fashion, in perturbation theory—see section 5), makes it clear that tuning of initial data provides the mechanism for making arbitrarily small black holes,

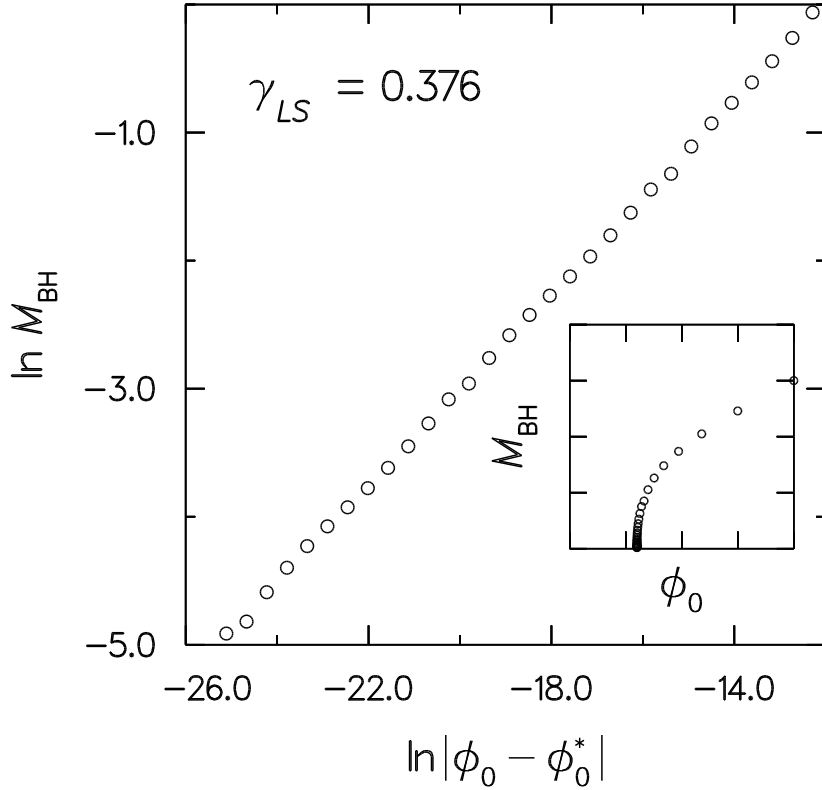


Figure 4. Typical evidence for mass scaling in the collapse of a massless scalar field. The data displayed here was generated from a one-parameter family of initially-ingoing Gaussian pulses of scalar field in which the overall amplitude of the pulse was varied. The mass-scaling exponent, $\gamma_{LS} \approx 0.376$, was determined from a least-squares fit. The inset clearly shows the “second order” (Type II) nature of the transition. It is worth noting that, particularly for compact pulse shapes such as the Gaussians used here, the mass scaling persists well out of the asymptotic regime, $p \rightarrow p^*$.

which in itself establishes that Type II transitions occur generically in the EMKG model. Direct measurement of the black hole masses in the super-critical regime provides additional evidence. One finds that, for a generic interpolating family $S[p]$, and as $p \rightarrow p^*$, the black hole masses are well-fit by a scaling law (see Figure 4):

$$M_{BH} = c_f |p - p^*|^\gamma, \quad (16)$$

where c_f is a family-dependent constant, but $\gamma = 0.37\dots$ is universal (i.e. family-independent).

As also noted in Figure 3, the nature of the critical solution immediately implies that the scalar curvature (see equation (13)) grows without bound near $r = 0$ in a precisely critical evolution. It is also clear from the simulations that these regions of arbitrarily high curvature are visible by observers at infinity. Indeed, the trailing edge of the scalar field pulse itself effectively does the job of tracking outwards propagating null geodesics emitted from the critical region. Again, the point is that, contrary to some expectations [13], without the formation of a horizon, one cannot indefinitely localize the mass-energy of the scalar field. Finally, I note that all of the above features of critical spherically-symmetric scalar collapse have been reproduced—using a variety of theoretical approaches and numerical techniques—by several other groups [13, 14, 15, 16].

3. Other Early Results in Critical Collapse

3.1. GRAVITATIONAL WAVE COLLAPSE

Shortly after the discovery of critical behaviour in the EMKG model, Abrahams and Evans [17] presented exciting results demonstrating that very similar effects occurred in the purely gravitational (i.e. vacuum) collapse of *axisymmetric* gravitational waves. Again, at least in principle, it is straightforward to construct interpolating families in this case, but, computationally, this problem is much more difficult to treat than the spherically symmetric EMKG system described above. Nonetheless, Abrahams and Evans were able to produce convincing evidence for (1) a discretely self-similar threshold solution, this time with $\Delta \approx 0.6$, and (2) mass-scaling in the super-critical regime, with $\gamma \approx 0.37$. The work in [17] used a single interpolating family; a follow-up paper [18] reported the observation of similar results from a second family, thus providing evidence for the universality of their critical solution.

3.2. RADIATION FLUID COLLAPSE

A third and very important example of critical behaviour came with the work by Evans and Coleman [19], who studied the spherically symmetric collapse of a perfect fluid with the simple equation of state

$$P = \frac{1}{3}\rho, \quad (17)$$

where P and ρ are the fluid's pressure and density respectively. Early on, Evans had realized that the self-similar nature of the Type II transitions

which were being observed could be used to great advantage in understanding what was happening in critical collapse. Familiar with the existence of continuously self-similar solutions in relativistic fluid flow, he argued that that the phase transition in the case of radiation fluid collapse should be characterized by continuous self-similarity. Proceeding from the *ansatz* of self-similarity, Evans and Coleman constructed a precisely self-similar solution and verified that it was identical to the critical solution generated from full dynamical evolution (again using interpolating families). Once more, convincing evidence for mass-scaling in the super-critical regime, with $\gamma \approx 0.36$, was found. Importantly, Evans also suggested that an investigation of the perturbative mode structure of the critical solution could provide the basis for the computation of the mass-scaling exponent. Finally, the apparent numerical equality of γ for the EMKG, vacuum axisymmetric and radiation fluid cases, led to a provocative, but short-lived conjecture, that there might be “true” universality of γ across various collapse models [19].

4. Self Similarity in Critical Collapse

As Evans anticipated, the self-similar nature of Type II critical solutions *has* proven crucial to our current understanding of black hole critical phenomena. Here I will only briefly sketch some key ideas concerning self-similarity in this context—the interested reader can consult Gundlach’s review [1] (and references contained therein) for a much more thorough presentation.

Restricting attention to spherical symmetry, we choose “geometric” coordinates, R and T , which are adapted to any particular critical solution. In the context of polar-radial gauge discussed above, obvious choices are $R \equiv r$ (areal radius) and $T \equiv (T_0^* - T_0)$, so that the $(0, 0)$ is the central singularity of the precisely critical solution, and time advances to the *past* of the singularity. The natural similarity variable (coordinate) for a type II critical solution is then

$$\zeta = \frac{R}{T}, \quad (18)$$

and one can use either T or R , or more conveniently, $\tau \equiv \ln T$ or $\rho \equiv \ln R$ as a second coordinate. Evolution along lines of constant ζ (see Figure 5) then represents evolution in scale. Continuously self-similar (CSS) solutions are characterized by

$$g(\zeta, \tau) = g(\zeta, \tau') \quad \tau, \tau' \text{ arbitrary}, \quad (19)$$

where g denotes any dynamical variable which exhibits scaling. Discretely self-similar (DSS) solutions, on the other hand, satisfy

$$g(\zeta, \tau) = g(\zeta, \tau \pm n\Delta) \quad n = 0, 1, 2, \dots, \quad (20)$$

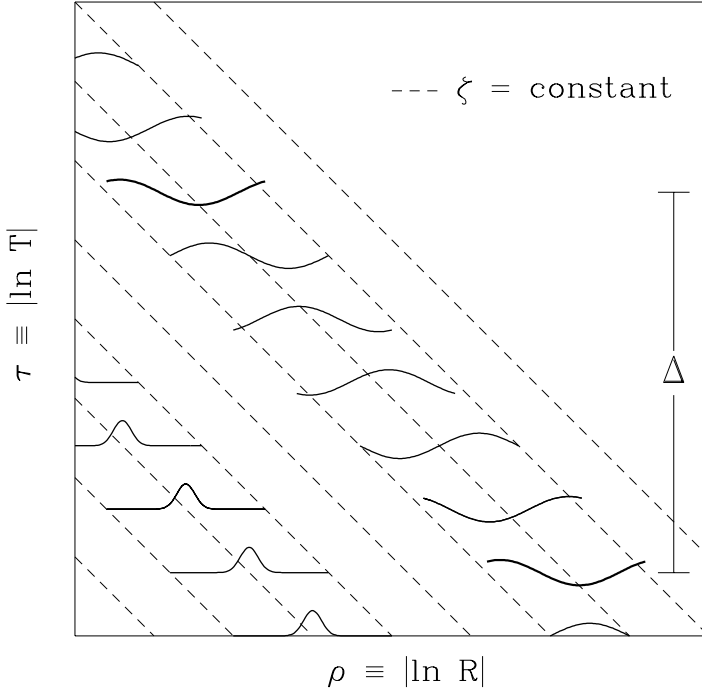


Figure 5. Schematic illustration of continuous (CSS) and discrete (DSS) self-similarity in critical collapse. The similarity variable $\zeta \equiv R/T$ is constant along dashed lines. In the case of CSS evolution (left part of the plot), a *single* critical profile propagates to the left (i.e. to smaller spatio-temporal scales), while in the DSS case, a non-trivial, but periodic, *sequence* of profiles, is generated. The periodicity in log-space, Δ , is a model-dependent (but initial-data-independent) scaling exponent.

where Δ is the model-dependent “echoing exponent”. It is important to note that, in both cases, the self-similar solution is *not* a complete spacetime, but (in R, T coordinates) a wedge-shaped region which, one expects, can be analytically continued (see [20, 21]) to produce a complete spacetime.

5. Perturbation Theory: Mode Structure of Critical Solutions

Again, as Evans suggested [19], the application of perturbation theory to black-hole threshold solutions has proven to be a powerful technique for studying and explaining many of the key features of critical collapse. Briefly, for any given collapse model (which includes specification of the matter content, coupling to gravity and other fields, symmetries, etc.), all of the current evidence suggests that one will find one or more isolated (in “initial-

data space") critical solutions, g^* . Operationally, g^* can be constructed either (1) indirectly, using the partial differential equations of motion and interpolating families of initial data, or (2) directly, starting from an *ansatz* which reflects the particular type of self-similarity exhibited by the critical solution.

Schematically (see [1] and [22] for more details), one then considers perturbations about the background, g^* , and looks for eigenmodes, $f_i(\zeta)$ with corresponding eigenvalues, λ_i , with the assumption that (small) departures, $\delta g(\zeta, \tau)$, from the critical solution can be then be expressed as

$$\delta g(\zeta, \tau) \equiv g(\zeta, \tau) - g^*(\zeta, \tau) = \sum_i C_i \exp(\lambda_i \tau) f_i(\zeta), \quad (21)$$

where the C_i are coefficients.

In terms of explaining the mass-scaling and universality of the Type II transitions discussed above, the crucial observation was made by Koike, Hara and Adachi [23], who noted that the “sharp” nature of the transition (as well as the universality) strongly suggested that of all the modes, only *one*, f_* , has an associated eigenvalue, λ_* with

$$\operatorname{Re} \lambda_* > 0. \quad (22)$$

That is, *there is only one growing mode associated with the critical solution*—all other modes generically die off as the critical solution is approached. It is then a straightforward matter of linearization of (21) and dimensional analysis to show that the black hole mass will satisfy a scaling law

$$M_{\text{BH}} \propto |p - p^*|^{1/\operatorname{Re} \lambda_*}, \quad (23)$$

so that

$$\gamma = \frac{1}{\operatorname{Re} \lambda_*}. \quad (24)$$

This argument provides an immediate and intuitive explanation for the observed universality (initial-data independence) of the Type II critical solutions—in tuning the family parameter, p , to the threshold value p^* , one is effectively tuning out the unstable mode in the initial conditions, so that as $p \rightarrow p^*$, the strong-field dynamics is well-described by the precisely critical solution over more and more decades of scale. Moreover, the eventual departure from g^* in any specific computation (sub-critical or super-critical) is well-approximated by

$$\delta g(\zeta, \tau) \sim \exp(\lambda_* \tau) f_*(\zeta), \quad (25)$$

independently of any specifics of the initial data. Thus, although Type II critical solutions are clearly unstable, they are, in some sense, the *least*

unstable solutions possible, by virtue of the fact that they possess only a single growing mode.

Koike *et al* tested their ideas in the context of the radiation fluid critical solution, found strong evidence that there *was* only one growing mode in perturbation theory, and from the eigenvalue of the mode, computed a scaling exponent, $\gamma = 0.3558\dots$ in excellent agreement with the Evans and Coleman simulations. Concurrent with [23], Maison [24] presented similar calculations which were, moreover, generalized to the case

$$P = k\rho \quad 0.01 \leq k \leq 0.888. \quad (26)$$

His specific results for $k = 1/3$ were in precise agreement with Koike *et al*, and, moreover, his general results clearly showed that the mass-scaling exponent was dependent on k —ranging from $\gamma = 0.114$ for $k = 0.01$ to $\gamma = 0.852$ for $k = 0.888$. This, of course, provided strong evidence for the model-*dependence* (i.e. “non-universality”) of γ .

The picture of Type II critical solutions as “intermediate attractors” [25] with 1-dimensional unstable manifolds has now been validated for many spherically symmetric models, including axion/dilaton collapse [26, 27] (see also [28] for dynamical evolutions in a generalized setting), the EMKG model [20, 29], the SU(2) Einstein-Yang-Mills model briefly discussed below [30], and scalar electrodynamics [31]. In the last case, Gundlach and Martin-Garcia also predicted an additional scaling law for the (scalar) charge of black holes, which was very quickly observed in independent work by Hod and Piran [16].

In addition to the critical solutions with one unstable mode described above, other self-similar, strong field solutions have been constructed and investigated (see for example, the work by Hirschmann and Eardley [21, 32]). It seems reasonable to assume that such solutions also sit at the black hole threshold, but they generically have two or more growing modes, so will *not* be intermediate attractors for *generic* 1-parameter interpolating families. However, there is evidence [33] that at least some of these solutions may be constructed via carefully constructed families of initial data.

Gundlach’s perturbative analysis of the EMKG system [20] also lead him to predict the existence of a universal “wiggle” in the mass-scaling law (16). Hod and Piran presented similar arguments and numerical evidence for the oscillation in [15]. It is probable that this wiggle is visible in Figure 4, but the systematic errors in the finite-difference computations which produced those results preclude a definitive statement.

Finally in interesting recent work, Garfinkle [34] considered the separation of Einstein’s equations into pieces governing (1) the dynamics of the overall scale of a self-gravitating system, and (2) the dynamics of the “scale invariant” part of the metric. As part of his study he constructed a model

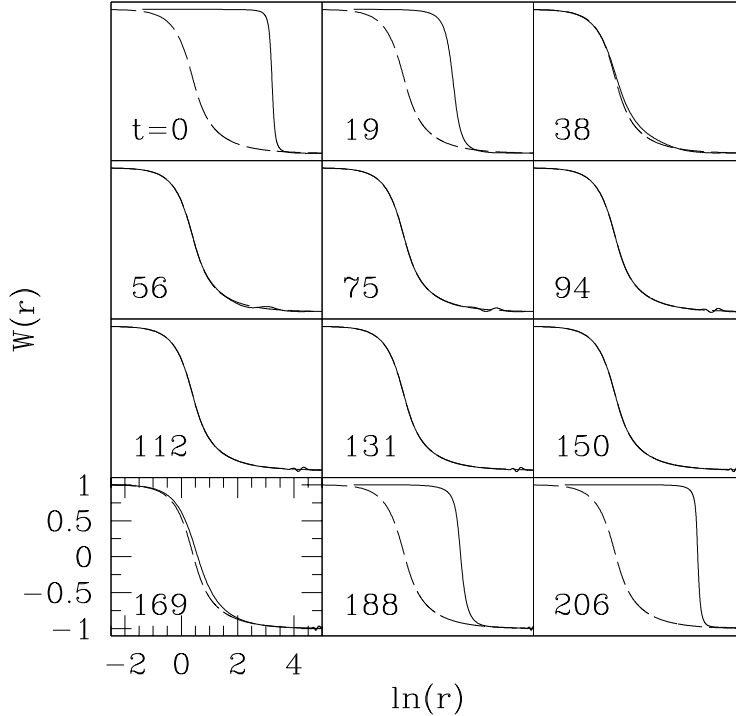


Figure 6. Evolution of the Yang-Mills potential, $W(r)$, in a near-critical evolution at the Type I transition in Einstein-Yang-Mills collapse. Solid lines show the dynamical evolution of $W(r)$, while the dashed lines superimpose the static, $n = 1$, Bartnik-McKinnon solution. The initial data is an incoming “kink” which implodes to the center (frames 1-3), sheds off Yang-Mills radiation and asymptotes to the static solution (frames 4-9). Because this evolution is sub-critical, the static configuration then completely disperses (frames 10-12) leaving flat spacetime behind. In a marginally super-critical case, a black hole containing essentially all of the mass of the static solution will form.

non-linear dynamical system (with three continuous degrees of freedom) which exhibited many of the features seen in Type II critical collapse.

6. Type I Behaviour: Einstein-Yang-Mills Collapse

In contrast to the recently discovered Type II transitions, Type I black-hole transitions are, of course, very familiar to astrophysicists in the context of the instability which generically arises in sequences of static stellar models parametrized, for example, by central density. A somewhat different Type I transition has recently been observed in the spherically symmetric collapse of an $SU(2)$ Yang-Mills field [35]. The equations of motion for this system are very similar to those for the EMKG model, with a single function,

$W(r, t)$ (the “Yang-Mills potential”) playing the role of the scalar field. However, largely due to the non-trivial vacuum structure of the theory, the phenomenology here is richer than in the scalar case. In particular, Bartnik and Mckinnnon [36] showed that the Einstein-Yang-Mills (EYM) model admits a countable infinity of regular, static solutions, conveniently labeled by the number, n , of zeros of the static profile $W_n(r)$ (W must be ± 1 at the origin and at infinity).

All of the Bartnik-Mckinnnon solutions, which may be viewed as resulting from a balance between the attractive gravitational interaction and the repulsive YM self-interaction, were soon demonstrated to be unstable [37], and, in fact, within the specific *ansatz* in which they were originally constructed, were shown to have precisely n unstable modes. This suggested to Bizoń that the $n = 1$ solution could be constructed as a Type I critical solution from the dynamical evolution of suitably constructed one-parameter families of initial data. This indeed turned out to be the case [35], and Figure 6 shows the evolution of a configuration near the Type I transition. As with the Type II solutions described above, the critical solution here has exactly one unstable mode in perturbation theory—tuning of initial data controls the effective level of that mode in the initial data, and as one approaches the critical point, the unstable $n = 1$ Bartnik-Mckinnnon solution persists for a proper time

$$T \sim -\sigma \ln |p - p^*|, \quad (27)$$

where in complete analogy to the Type II analysis, the scaling exponent, σ , is simply the reciprocal of the real part of the eigenvalue corresponding to the unstable mode.

Interestingly, Type II behaviour is also seen in the EYM model [35] with $\Delta = 0.74$ and $\gamma = 0.20$, providing rather definitive evidence of the non-universality of mass-scaling exponents. Furthermore, considering suitable two-parameter families of solutions, $\mathcal{S}[p_1, p_2]$, one generically finds a co-existence point of the two types of threshold behaviour in the (p_1, p_2) plane. Phenomena analogous to all those described in this section have also been recently reported by Brady, Chambers and Goncalves [38] in the context of the collapse of a *massive* scalar field.

7. An Irregular Critical Solution

A final and novel example [39] of black-hole critical behaviour is provided by a family of solutions (family parameter ϵ) of the EMKG system which has been independently discovered over the years by many authors [40, 41, 42], most recently by van Putten [43]. These solutions are spherically-symmetric and static, with an irregular origin, and have the feature that as the adjustable parameter ϵ is tuned to 0, the region of spacetime exterior to

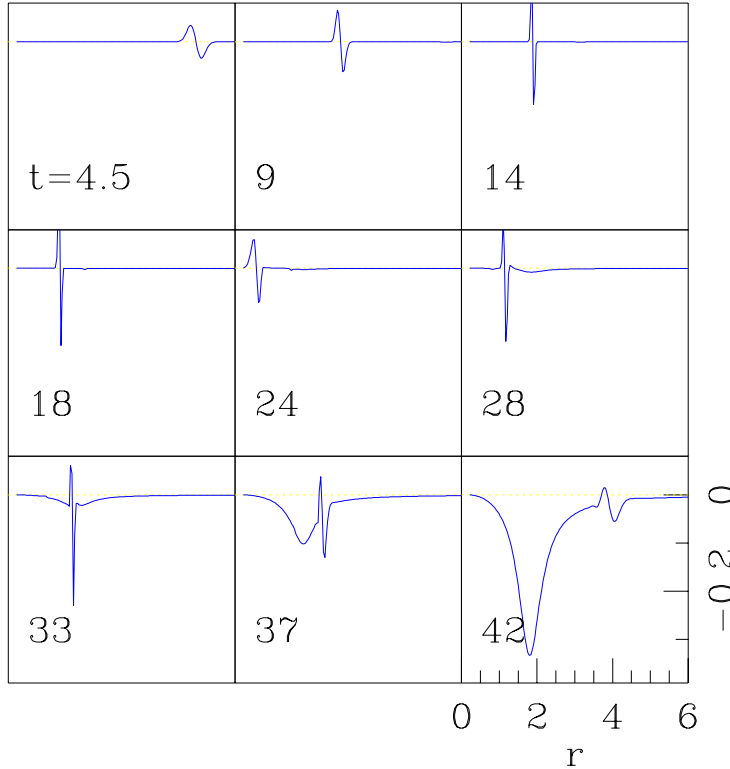


Figure 7. Excitation of the growing mode of the static, irregular scalar field critical solution found by various authors [40,41,42], and recently discussed by van Putten [43]. Here, the dynamical evolution of the quantity $ra\alpha^{-1}\partial\phi/\partial t$, which vanishes for the static solution, is plotted. The initial data contains a perturbation in the scalar field, which travels inward, bounces off the irregular origin between $t = 18$ and $t = 28$, then escapes to infinity. As it propagates through the region of the spacetime corresponding to the near-horizon region in a Schwarzschild spacetime, the perturbing pulse excites the single, growing mode of the static solution. Through judicious choice of perturbations, the growing mode can be excited with either sign—one sign leads to black hole formation, the other apparently leads to dispersal. Also note the blue-shifting and red-shifting of the perturbation (indicative of the strong-field nature of the static solution) as it travels inwards and outwards respectively.

the effective support of the scalar field becomes a better and better approximation of the Schwarzschild geometry. However, none of the solutions exhibit event horizons, and because of the difficulty in numerically treating horizon-containing spacetimes, van Putten proposed that the solutions

might be useful for “mocking up” black holes. Unfortunately (from the point of view of that proposal), the solutions are unstable, and thus likely to be of little use as “approximate black holes”. However, as with the other threshold solutions described above, these solutions appear to be minimally unstable—that is, they seem to have a single unstable eigenmode in perturbation theory and, furthermore (see Figure 7), appear to sit at the threshold of black hole formation.

8. Angular Momentum in Critical Collapse

Very recent work by Gundlach [44, 45] addresses the important issue of the role of angular momentum at the threshold of black hole formation. In [44], non-spherical perturbations about the spherically-symmetric Evans-Coleman radiation-fluid ($P = \rho/3$) critical solution are considered, with the conclusion that there are *no* growing non-spherical modes. This strongly suggests that, at least for small departures from spherical symmetry, the Evans-Coleman solution will persist at the black hole threshold. In [45] Gundlach investigates the dominant non-spherical mode ($\ell = 1$), which contributes to the angular momentum L of the system and predicts that the overall amplitude of the spin should scale as

$$L \propto |p - p^*|^\mu, \quad (28)$$

with $\mu \approx 0.80$, but also that the spin vector will rotate in space as a function of $p - p^*$, with a universal frequency $\omega \approx 0.23$. It will be extremely interesting to investigate these predictions, and related issues, using full simulations in axisymmetry.

9. Quantum Mechanical Effects

The nature of Type II critical solutions—particularly the fact that they describe strong-field, gravitationally-mediated dynamics down to arbitrarily small scales—makes it natural to study the impact of matter-quantization on criticality. At the current time, the overall picture is murky, even given the restriction to semi-classical approaches. Here, there are at least two heuristic viewpoints. On the one hand, quantization will generally introduce a length scale to the otherwise scale-free dynamics at a Type II threshold. Thus, one might expect a mass gap to appear at threshold, and there is some evidence [46, 47, 48] for this. On the other hand, the predominant semi-classical effect which will be encountered is probably Hawking radiation, which, one could argue, should merely “renormalize” the classical competition in the model, suggesting that the transition remains Type II [49, 50]. Despite the current confusion, one thing does seem clear—because Type

II solutions are naturally strong-field on arbitrarily small scales, they *demand* to be quantized in a way that the Schwarzschild solution, for example (where one must go in and, by hand, tune M to zero to achieve unbounded curvatures) does not.

10. Conclusions

In a few short years, the study of the threshold of black hole formation has developed into an active and (at least to some of us!) exciting sub-field of relativity. Although the initial results are now fairly well understood, it is clear that there remains an extremely rich phenomenology waiting to be explored, particularly in the context of non-spherically-symmetric collapse. The reader may rest assured that vigorous efforts to explore this new territory are currently underway.

11. Acknowledgements

It is a pleasure to thank my collaborators S.L. Liebling, E.W. Hirschmann, P. Bizo  and T. Chmaj. The financial support of NSF PHY9722068 and a Texas Advanced Research Project grant is also gratefully acknowledged. Finally, I wish to thank the conference organizers for their substantial efforts in putting together such a wonderful meeting.

References

1. Gundlach, C. (1997), *gr-qc/9712084*.
2. Evans, C.R. (1993), in *Proceedings of General Relativity and Gravitation 1992*, eds. Gleiser R.J. *et al.*, 41.
3. Eardley, D.M. (1993), *Ann. N. Y. Acad. Sci.*, **688**, 408.
4. Wald, R.M. (1997), *gr-qc/9710068*.
5. Christodoulou, D. (1987), *Commun. Math. Phys.*, **109**, 613; (1991) *Commun. Pure & App. Math.*, **44**, 339; (1991) *Commun. Pure & App. Math.*, **46**, 1131; (1994) *Ann. Math.*, **140**, 1994; (1998) *Ann. Math.*, (in press).
6. Goldwirth, D. and Piran, T. (1987), *Phys. Rev.*, **D36**, 3575.
7. Choptuik, M.W. (1986), Ph. D. Thesis, University of British Columbia (unpublished).
8. Choptuik, M.W. (1989), in *Frontiers in Numerical Relativity*, eds. C.R. Evans *et al.*, 206.
9. Christodoulou, D. (1987), personal communication.
10. Choptuik, M.W. (1992), in *Approaches to Numerical Relativity*, ed. R. d'Inverno, 202.
11. Choptuik, M.W. (1993), *Phys. Rev. Lett.*, **70**, 9.
12. Choptuik, M.W. (1994), in *Deterministic Chaos in General Relativity*, eds. D. Hobill *et al.*, 155.
13. Hamade, R.S. and Stewart, J.M. (1996) *Class. and Quant. Grav.*, **13**, 497.
14. Garfinkle, D. (1995), *Phys. Rev.*, **D51**, 5558.
15. Hod, S. and Piran, T. (1997), *Phys. Rev.*, **D55**, 440.
16. Hod, S. and Piran, T. (1997), *Phys. Rev.*, **D55**, 3485.

17. Abrahams, A.M. and Evans, C.R. (1993), *Phys. Rev. Lett.*, **70**, 2980.
18. Abrahams, A.M. and Evans, C.R. (1993), *Phys. Rev.*, **D49**, 3998.
19. Evans, C.R. and Coleman, J.S. (1994), *Phys. Rev. Lett.*, **72**, 1782.
20. Gundlach, C. (1997), *Phys. Rev.*, **D55**, 695.
21. Hirschmann, E. W. and Eardley, D. M. (1995), *Phys. Rev.*, **D51**, 4198.
22. Hara T., Koike T. and Adachi. S. (1996), [gr-qc/9607010](#).
23. Koike, T., Hara. T., and Adachi. S. (1995), *Phys. Rev. Lett.*, **74**, 5170.
24. Maison, D. (1995), *Phys. Lett.*, **B366**, 82.
25. Barenblatt, G.I. (1979), *Similarity, Self-Similarity, and Intermediate Asymptotics*, Consultants Bureau.
26. Eardley D., Hirschmann. E.W. and Horne, J. (1995) *Phys. Rev.*, **D52**, 5397.
27. Hamade, R.S., Horne, J.H. and Stewart, J.M. (1996) *Class. and Quant. Grav.*, **13**, 2241.
28. Liebling, S.L. and Choptuik, M.W. (1996) *Phys. Rev. Lett.*, **77**, 1424.
29. Gundlach, C. (1995), *Phys. Rev. Lett.*, **75**, 3214.
30. Gundlach, C. (1997), *Phys. Rev.*, **D55**, 6002.
31. Gundlach, C. and Martin-Garcia, J.M. (1997), *Phys. Rev.*, **D54**, 7353.
32. Hirschmann, E. W. and Eardley, D. M. (1995), *Phys. Rev.*, **D52**, 5850.
33. Liebling, S.L. (1998), Ph. D. Thesis, UT Austin (unpublished).
34. Garfinkle, D. (1997), *Phys. Rev.*, **D56**, 3169.
35. Choptuik, M.W., Chmaj, T. and Bizoń. P. (1996), *Phys. Rev. Lett.*, **77**, 424.
36. Bartnik, R. and Mckinnon, J. (1988), *Phys. Rev. Lett.*, **61**, 141.
37. Straumann, N. and Zhou, Z. (1990), *Phys. Lett.*, **B237**, 353.
38. Brady, P., Chambers C.M. and Goncalves S.M.C.V (1997), *Phys. Rev.*, **D56**, 6057.
39. Choptuik, M.W., Liebling, S.L. and Hirschmann. E.W. (1997), *Phys. Rev.*, **D55**, 6014.
40. Buchdahl, H.A. (1959), *Phys. Rev.* **115**, 1325.
41. Brans, C. and Dicke, R.H. (1961), *Phys. Rev.* **124**, 925.
42. Janis, A.I., Newman, E.T. and Winicour, J. (1968), *Phys. Rev. Lett.*, **20**, 878.
43. van Putten, M.H.P.M. (1996), *Phys. Rev.*, **D54**, R5931.
44. Gundlach, C. (1997), [gr-qc/9710066](#).
45. Gundlach, C. (1997), [gr-qc/9711079](#).
46. Chiba, T. and Siino, M. (1997), *Mod. Phys. Lett.*, **A12**, 709.
47. Bose, S., Parker, L. and Peleg, Y. (1996), *Phys. Rev.*, **D54**, 7490.
48. Peleg, Y., Bose, S. and Parker, L. (1997), *Phys. Rev.*, **D55**, 4525.
49. Strominger, A. and Thorlacius, L. (1994), *Phys. Rev. Lett.*, **72**, 1584.
50. Ayal, S. and Piran, T. (1997), *Phys. Rev.*, **D56**, 4768.